PHYSICAL REVIEW C **85**, 044320 (2012)

Breaking of $N = 8$ magicity in ^{13}Be

Yoshiko Kanada-En'yo
Department of Physics, Kyoto University, Kyoto 606-8502, Japan
(Received 8 March 2012; revised manuscript received 2 April 2012; published 24 April 2012)

The structure of ^{13}Be was investigated with antisymmetrized molecular dynamics. The variation after spin and parity projections was performed. An unnatural parity $1/2^-$ state was suggested to be lower than the $5/2^+$ state indicating that vanishing of the $N = 8$ magic number occurs in ^{13}Be. A low-lying $3/2^+$ state with a $2\hbar\omega$ configuration was also suggested. Developed cluster structures were found in the intruder states. The lowering mechanism of the intruder states was discussed in terms of molecular orbitals around a 2α core.

DOI: 10.1103/PhysRevC.85.044320 PACS number(s): 21.10.−k, 21.60.−n, 27.20.+n

I. INTRODUCTION

One of the exotic phenomena discovered in unstable nuclei is the vanishing of neutron magic numbers. In neutron-rich Be isotopes, the breaking of $N = 8$ magicity in ^{11}Be has been known from the abnormal spin and parity $1/2^+$ of the ground state. The vanishing of the $N = 8$ magic number in ^{12}Be has been suggested by slow β decay to ^{12}B [1] and it has been supported by various experiments [2–6]. The $N = 8$ shell breaking has been suggested also in ^{11}Li by experimental and theoretical works [7]. Even though ^{12}Be and ^{11}Li are neighboring nuclei, they have different characters and the shell breaking mechanism is not the same between the two nuclei. One of the remarkable features of ^{12}Be different from ^{11}Li is the developed cluster structure, which plays an important role in the shell breaking in Be isotopes.

Cluster structures of Be isotopes have been intensively investigated in many theoretical works [8–29]. Low-lying states in neutron-rich Be were described successfully with cluster models and molecular-orbital models assuming two α clusters and surrounding neutrons. The formation of a 2α core in Be isotopes was confirmed by the author and her collaborators with a method of antisymmetrized molecular dynamics which does not rely on *a priori* assumption of any clusters [14–19]. These works revealed that 2α structures are favored in neutron-rich Be isotopes where valence neutrons around the 2α core play important roles. To understand cluster features of low-lying states of neutron-rich Be, a molecular orbital picture is helpful [8–13]. In the picture, molecular orbitals are formed by a linear combination of p orbits around two α clusters, and valence neutrons occupy the molecular orbitals. A longitudinal positive-parity orbital is called a "$\sigma_{1/2}$ orbital". Since the $\sigma_{1/2}$ orbital has two nodes along the α-α direction, it gains kinetic energy as the 2α cluster develops. Note that the $\sigma_{1/2}$ orbital corresponds to the "$1/2[220]''$ orbit in the Nilsson model (a deformed shell model) [30] and it originates in the sd orbit in the spherical shell model limit. In the molecular orbital picture, the ground states of ^{11}Be and ^{12}Be are regarded as the configurations with one and two neutrons in the $\sigma_{1/2}$ orbital, respectively, which correspond to the intruder configurations in terms of the spherical shell model. In other words, the lowering mechanism of the intruder states in Be isotopes can be understood by the the energy gain of the $\sigma_{1/2}$ orbital in the developed 2α cluster structure.

It is then a challenging issue to investigate cluster features and shell evolution in further neutron-rich Be isotopes near the drip line. Indeed, many experiments have been performed to observe energy spectra of ^{13}Be (see Refs. [31,32] and references therein). Since ^{13}Be is an unbound nucleus, all energy levels are resonance states. A resonance about 2 MeV above the neutron-decay threshold has been observed in several experiments and it has been assigned to a $5/2^+$ state [31–38]. However, other levels of ^{13}Be have not been confirmed yet. The position of a $1/2^-$ state relative to the $5/2^+$ state is, in particular, a key problem concerning the breaking of $N = 8$ magicity. Understanding of low-energy spectra measured with invariant mass measurements of $^{12}\mathrm{Be} + n$ is controversial. Some works argued that observed low-energy spectra just above the $^{12}\mathrm{Be} + n$ threshold are described by the contribution of a s-wave virtual or resonance state [31,36,38]. For the threshold strength in $^{12}\mathrm{Be} + n$ invariant mass spectra in break-up reactions, a possible artifact from the decay of $^{14}\mathrm{Be}^*(2^+)$ was suggested [39]. On the other hand, Kondo *et al.* reported the existence of a p-wave resonance in the low-energy peak below the $5/2^+$ state and tentatively assigned it to a $1/2^-$ state suggesting the breaking of $N = 8$ magicity in ^{13}Be. However, a controversial claim was given [40], and the energy position of the $1/2^-$ state is still under discussion.

If the inversion of single-particle levels does not occur in ^{13}Be, the unnatural-parity $1/2^-$ state should be higher than natural-parity $1/2^+$ and $5/2^+$ states. The question is whether or not the inversion occurs and the $1/2^-$ state comes down to the low-energy region in ^{13}Be. Provided that the inversion occurs, cluster structure may play an important role in the intruder $1/2^-$ state as well as ^{11}Be and ^{12}Be. Some theoretical calculations suggested the possibility of a low-lying $1/2^-$ state in ^{13}Be [32,41]. For instance, a shell model calculation for ^{13}Be using the SFO interaction [42], which is adjusted to reproduce the parity inversion of ^{11}Be, gives the $1/2^-$ ground state in ^{13}Be [32]. In microscopic cluster model calculations, there are only a few applications to ^{13}Be [43] because of the large number of valence neutrons.

Our aim is to investigate the structure of ^{13}Be. A method of energy variation after spin-parity projection (VAP) in the framework of antisymmetrized molecular dynamics (AMD) [14,16,44] is applied to ^{13}Be. The AMD + VAP method has been already applied for studying ^{10}Be [17], ^{11}Be [18], and ^{12}Be [19] and successfully described properties

of ground and excited states. In the energy levels of ^{13}Be calculated by using the interaction that reproduces the parity inversion of ^{11}Be, we will suggest a low-lying $1/2^-$ state below the $5/2^+$ state. We show the coexistence of $0\hbar\omega$, $1\hbar\omega$, and $2\hbar\omega$ states in a low-energy region of ^{13}Be and suggest the breaking of $N = 8$ magicity. We discuss cluster structures of ^{13}Be and indicate that the calculated states of ^{13}Be can be classified by molecular orbital configurations. The neutron shell breaking is discussed systematically in a chain of Be isotopes focusing on cluster aspect.

This paper is organized as follows. In the next section, the formulation of the present calculation is explained. The results are shown in Sec. III and discussions are given in Sec. IV. Finally, in Sec. V, a summary and an outlook are given.

II. FORMULATION

We describe ^{13}Be with AMD wave functions by applying the VAP method. For the AMD + VAP method, the reader is referred to Refs. [17–19,45]. The method is basically the same as those applied to ^{10}Be, ^{11}Be, and ^{12}Be. One difference in calculation procedures from Refs. [17–19] is that we do not adopt an artificial barrier potential in the present calculation which was used in the previous works. To see the effects of quasibound features of the last valence neutron on energy spectra, we also adopt $^{12}\mathrm{Be} + n$ wave functions by using the ^{12}Be core wave functions obtained with AMD + VAP for ^{12}Be.

A. AMD wave functions

An AMD wave function is given by a Slater determinant of Gaussian wave packets:

$$\Phi_{\mathrm{AMD}}(\mathbf{Z}) = \frac{1}{\sqrt{A!}}\mathcal{A}\{\varphi_1, \varphi_2, ..., \varphi_A\}, \tag{1}$$

where the ith single-particle wave function is written by a product of spatial (ϕ), intrinsic spin (χ), and isospin (τ) wave functions as

$$\varphi_i = \phi_{\mathbf{X}_i}\chi_i\tau_i, \tag{2}$$

$$\phi_{\mathbf{X}_i}(\mathbf{r}_j) = \left(\frac{2\nu}{\pi}\right)^{4/3}\exp\left\{-\nu\left(\mathbf{r}_j - \frac{\mathbf{X}_i}{\sqrt{\nu}}\right)^2\right\}, \tag{3}$$

$$\chi_i = \left(\frac{1}{2} + \xi_i\right)\chi_\uparrow + \left(\frac{1}{2} - \xi_i\right)\chi_\downarrow. \tag{4}$$

$\phi_{\mathbf{X}_i}$ and χ_i are spatial and spin functions, and τ_i is the isospin function fixed to be up (proton) or down (neutron). Accordingly, an AMD wave function is expressed by a set of variational parameters, $\mathbf{Z} \equiv \{\mathbf{X}_1, \mathbf{X}_2, \cdots, \mathbf{X}_A, \xi_1, \xi_2, \cdots, \xi_A\}$. The width parameter ν is chosen to be $\nu = 0.17$ fm^{-2} which is the same value as that used for ^{12}Be in Ref. [19].

B. Variation after projection method

Energy variation after spin and parity projections (VAP) in the AMD model space is performed as is done in the previous studies of Be isotopes [17–19]. For the lowest J^π state, the parameters $\mathbf{X}_i$ and $\xi_i (i = 1 \sim A)$ are varied to minimize the energy expectation value of the Hamiltonian, $\langle\Phi|H|\Phi\rangle/\langle\Phi|\Phi\rangle$, with respect to the spin-parity eigenwave function projected from an AMD wave function; $\Phi = P^{J\pi}_{MK}\Phi_{\mathrm{AMD}}(\mathbf{Z})$. Here, $P^{J\pi}_{MK}$ is the spin-parity projection operator. The energy variation is performed with a frictional cooling method [16]. Then the optimum AMD wave function $\Phi_{\mathrm{AMD}}(\mathbf{Z}^{J^\pi})$, which approximately describes the intrinsic wave function for a J^π state, is obtained. For each $J^\pi = J^{\pi_\alpha}_\alpha$, the optimum parameters $\mathbf{Z}^{J_\alpha\pi_\alpha}$ are obtained. After the VAP procedure, final wave functions are calculated by superposing the spin-parity eigenwave functions projected from all the AMD wave functions $\Phi_{\mathrm{AMD}}(\mathbf{Z}^{J_\alpha\pi_\alpha})$ obtained by VAP for various $J^{\pi_\alpha}_\alpha$ states. Namely, the final wave functions for the J^π states are expressed as

$$|J^\pi\rangle = \sum_{\alpha,K} c^{J^\pi}(K, J_\alpha, \pi_\alpha)\left|P^{J\pi}_{MK}\Phi_{\mathrm{AMD}}\left(\mathbf{Z}^{J_\alpha\pi_\alpha}\right)\right\rangle, \tag{5}$$

where the coefficients $c^{J^\pi}(K, J_\alpha, \pi_\alpha)$ are determined by the diagonalization of norm and Hamiltonian matrices.

C. $^{12}\mathrm{Be} + n$ model

As will be shown later, the results obtained with AMD + VAP show that low-lying states of ^{13}Be can be interpreted as $^{12}\mathrm{Be} + n$, where the ^{12}Be core is the intrinsic state of the $^{12}\mathrm{Be}(0^+_1)$ having an intruder $2\hbar\omega$ configuration or that of $^{12}\mathrm{Be}(0^+_2)$ with a normal $0\hbar\omega$ configuration. In reality, ^{13}Be is an unbound nucleus and all states are resonances above the $^{12}\mathrm{Be} + n$ threshold. In such a case, asymptotic behavior of the valence neutron wave function in the outer region can be important, in particular, for energy position of low angular-momentum states. However, the AMD method is not suitable to describe detailed behaviors of asymptotic regions, because a system is expressed by a Slater determinant of Gaussians and is treated in a bound state approximation in the AMD model. To see effects from spatial extension of the last neutron on energies of resonances, we also calculate energy levels in a $^{12}\mathrm{Be} + n$ model described below.

In the $^{12}\mathrm{Be} + n$ model, we first apply AMD + VAP to ^{12}Be to obtain intrinsic wave functions $\Phi(^{12}\mathrm{Be} : 2\hbar\omega)$ of $^{12}\mathrm{Be}(0^+_1)$ and $\Phi(^{12}\mathrm{Be} : 0\hbar\omega)$ of $^{12}\mathrm{Be}(0^+_2)$ [19]. Each intrinsic wave function $\Phi(^{12}\mathrm{Be} : \alpha)$ ($\alpha = 0\hbar\omega, 2\hbar\omega$) is expressed by a AMD wave function and it is written by a Slater determinant. Then we add one neutron to the core wave functions $\Phi(^{12}\mathrm{Be} : 2\hbar\omega)$ and $\Phi(^{12}\mathrm{Be} : 0\hbar\omega)$. The additional neutron wave function in the $^{12}\mathrm{Be} + n$ system is described by a Gaussian wave packet located at a position $\mathbf{X}$ relative to the core. A ^{13}Be wave function for a J^π state is described by a linear combination of $^{12}\mathrm{Be} + n$ wave functions with various positions $\mathbf{X}$ as

$$\Psi^{J\pi} = \sum_\alpha \sum_{\sigma=\uparrow,\downarrow} \sum_k \sum_K \tag{6}$$

$$c^{J\pi}_{\alpha\sigma kK} P^{J\pi}_{MK}\mathcal{A}\left\{\Phi_{-\frac{\mathbf{x}_k}{13}}(^{12}\mathrm{Be} : \alpha)\psi_{n\sigma}\left(\frac{12}{13}\mathbf{X}_k\right)\right\}, \tag{7}$$

where $\psi_{n\uparrow(\downarrow)}(\mathbf{X})$ is a spin-up (spin-down) neutron wave function with a Gaussian form with the width ν parameter localized at $\mathbf{X}$:

$$\psi_{n\uparrow(\downarrow)}(\mathbf{X}) = \phi_{\mathbf{X}}\chi_{\uparrow(\downarrow)}, \tag{8}$$

$$\phi_{\mathbf{X}} = \left(\frac{2\nu}{\pi}\right)^{4/3} \exp\left\{-\nu\left(\mathbf{r} - \frac{\mathbf{X}}{\sqrt{\nu}}\right)^2\right\}. \tag{9}$$

The ^{12}Be wave function is shifted by $-\mathbf{X}_k/13$ to take into account the recoil effect from the last neutron. For the total wave function, the antisymmetrization and the spin-parity projection are performed as well as the superposition of basis wave functions.

In the present calculation, the intrinsic states $\Phi(^{12}\mathrm{Be} : \alpha)$ are deformed and their orientations are chosen to satisfy $\langle x^2\rangle \leqslant \langle y^2\rangle \leqslant \langle z^2\rangle$ and $\langle xy\rangle = \langle yz\rangle = \langle zx\rangle = 0$. For the position $\mathbf{X}_k$ of the last neutron Gaussian wave function, grid points in the $|x| \leqslant 5$ fm and $|z| \leqslant 5$ fm regions on the $y = 0$ plane are taken. The grid spacing is chosen to be 1 fm.

When an intrinsic wave function of the ^{12}Be core is axial symmetric, $\mathbf{X}_k$ on the y plane is enough to take into account the coupling of the last neutron with all rotational band members of ^{12}Be constructed from the intrinsic wave function. Strictly speaking, the present ^{12}Be wave functions are not axial symmetric, however, $\mathbf{X}_k$ is restricted only on the $y = 0$ plane to save numerical cost in the present calculation.

With the $^{12}\mathrm{Be} + n$ model, we calculate ^{13}Be energy spectra. Comparing the $^{12}\mathrm{Be} + n$ model calculation with the AMD + VAP one, we will discuss, in particular, how the energy spectra can be modified from the AMD + VAP results by improving the last neutron wave function.

III. RESULTS

A. Effective interaction

We used the same effective nuclear interaction as that used in Refs. [18,19]. It is the MV1 force [46] for the central force supplemented by a two-body spin-orbit force with the two-range Gaussian form the same as that in the G3RS force [47]. The Coulomb force is approximated using a seven-range Gaussian form. We adopted the interaction parameters that are used for ^{11}Be and ^{12}Be [18,19]. Namely, the Majorana, Bartlett, and Heisenberg parameters in the MV1 force are $m = 0.65$, $b = 0$, and $h = 0$, respectively, and the spin-orbit strengths are taken to be $u_I = -u_{II} = 3700$ MeV. We denote this parametrization by the set (1) interaction. To see the interaction dependence of the theoretical results, we also used the other parametrization (2) with weaker spin-orbit forces, $u_I = -u_{II} = 2500$ MeV.

The energy levels of the excited states of ^{10}Be, ^{11}Be, and ^{12}Be are reproduced well by the AMD + VAP calculations with the set (1) interaction. Particularly, the breaking of the $N = 8$ magicity in ^{11}Be and ^{12}Be are successfully described with the set (1) interaction [18,19]. In this paper, we mainly discuss the results calculated with set (1).

B. Energy levels

We applied AMD + VAP to ^{13}Be and calculated J^π states up to $J = 5/2$. The calculated energy levels of ^{13}Be are shown in Fig. 1 compared with experimental energy levels reported in Ref. [32]. Energy levels of ^{11}Be are also shown. As mentioned in Ref. [18], the set (1) interaction reproduces the unnatural parity ground state $1/2^+$ in ^{11}Be, while the set (2) interaction fails to describe the parity inversion.

In the result with the set (1) interaction, energy levels of ^{13}Be are found to be out of the normal ordering. $1/2^-$ and $3/2^+$ states almost degenerate at the lowest energy and a $5/2^+$ state exists above them. As will be discussed later, the $1/2^-$ and $3/2^+$ states have dominantly $1\hbar\omega$ and $2\hbar\omega$ excited configurations, respectively, while the $5/2^+$ state is described by a normal $0\hbar\omega$ configuration. The appearance of these intruder states in such a low-energy region suggests the breaking of $N = 8$ magicity in ^{13}Be as well as ^{11}Be.

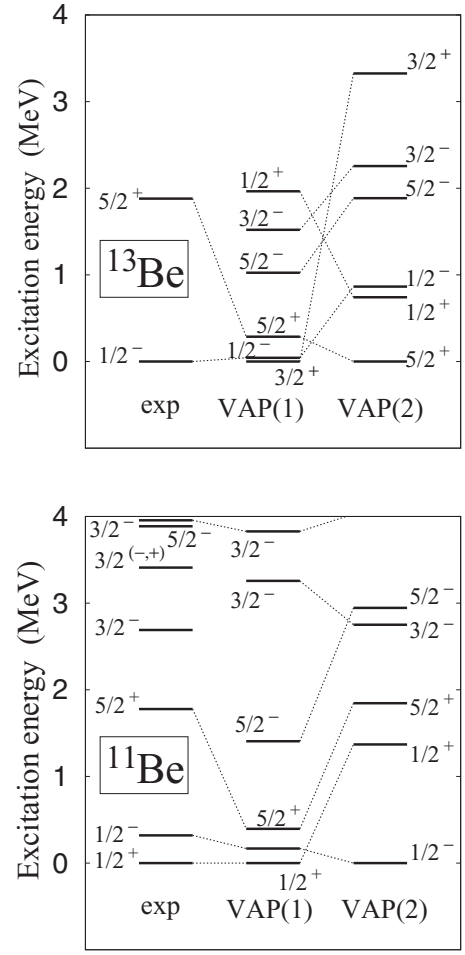

FIG. 1. Energy levels of (upper) ^{13}Be and (lower) ^{11}Be. Excitation energies are shown. The calculated levels are obtained with AMD + VAP by using the set (1) and (2) interactions. For ^{11}Be, the results calculated with AMD + VAP are taken from [18] and the experimental data are from [48]. The experimental data of ^{13}Be are those in Ref. [32].

In contrast, in the result with the set (2) interaction, the $5/2^+$ state is the lowest and the $1/2^-$ and $3/2^+$ states are higher than it as naively expected from the spherical shell model.

Although all states are resonances above the $^{12}\mathrm{Be}+n$ threshold in a real ^{13}Be system, they are treated in a bound state approximation in the present AMD + VAP calculation. In principle, a resonance energy might decrease when the last neutron occupies a low angular-momentum orbit because of an extended neutron wave function in an outer region. It means that asymptotic behavior of the valence neutron should be taken into account carefully for a more detailed discussion of energy levels. To see how the level ordering is affected by improving wave functions for the last neutron, we calculated energy levels of ^{13}Be also in the $^{12}\mathrm{Be}+n$ model.

The ^{13}Be energy spectra calculated with the $^{12}\mathrm{Be}+n$ model by using the set (1) interaction are shown in Fig. 2. The calculated energies are measured from the theoretical value -61.3 MeV of the ^{12}Be-n threshold energy, which is evaluated by diagonalizing spin-parity eigenstates projected from $\Phi(^{12}\mathrm{Be}:2\hbar\omega)$ and $\Phi(^{12}\mathrm{Be}:0\hbar\omega)$. For all states, the $^{12}\mathrm{Be}+n$ model calculation gives about a few MeV lower energies than those obtained with AMD + VAP because of improving neutron wave functions. The level ordering somehow changes from the VAP results, for instance, the $3/2^+$ state shifts up while the $1/2^+$ state comes down relatively. However, the $^{12}\mathrm{Be}+n$ calculation shows again the feature of the neutron magic number breaking that various spin and parity states degenerate in the low energy region. In particular, it should be pointed that the $1/2^-$ state is the lowest, consistent with the experimental report by Kondo *et al.* [32]. The calculated level structure, however, does not sufficiently agree with the experimental data. A possible assignment of calculated levels to experimental ones will be mentioned in the next section.

In experimental and theoretical studies of ^{13}Be, the $1/2^+$ state has been suggested to be a virtual state and contribute to the spectra near the $^{12}\mathrm{Be}+n$ threshold energy [31,32,43]. In the present calculation, model space is not enough to describe

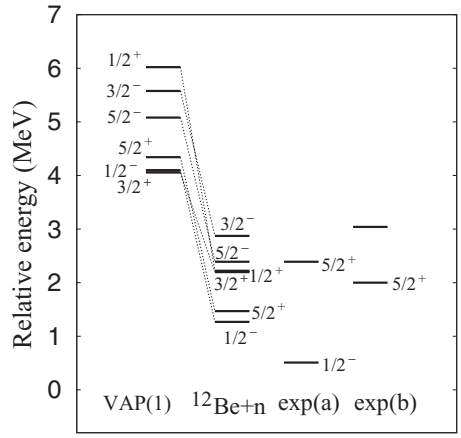

FIG. 2. Energy levels of ^{13}Be calculated with AMD + VAP and those with the $^{12}\mathrm{Be}+n$ model by using the set (1) interaction. Energies relative to the ^{12}Be-n threshold are shown. The calculated energies are measured from the theoretical ^{12}Be-n threshold energy, -61.3 MeV. Experimental energies are those taken from (a) Refs. [32] and (b) [31].

a virtual state. That may be the reason why the $1/2^+$ state is still higher than the $1/2^-$ and $5/2^+$ states even in the $^{12}\mathrm{Be}+n$ model calculation.

IV. DISCUSSIONS

In the present AMD + VAP calculation, any clusters are not assumed in the model. Nevertheless, the results suggest that cluster structures appear in ^{13}Be as well as other Be isotopes. Moreover, the ^{13}Be states obtained with AMD + VAP can be associated with $^{12}\mathrm{Be}+n$ states, and their structures correspond to those of the $^{12}\mathrm{Be}+n$ model calculation. Since each intrinsic wave function obtained by AMD + VAP is expressed with a single Slater determinant, AMD + VAP wave functions are useful to analyze intrinsic structures. We here discuss cluster features of ^{13}Be by investigating AMD + VAP wave functions while focusing on the 2α cluster and valence neutron configurations. We also discuss systematics of low-lying states in neutron-rich Be isotopes in the molecular orbital picture.

A. Intrinsic structures and clustering

As seen in density distributions of intrinsic wave functions shown in Fig. 3, a 2α core is formed in ^{13}Be. In particular, developed 2α cluster structures with large deformations are found in negative-parity states, $^{13}\mathrm{Be}(1/2^-)$, $^{13}\mathrm{Be}(3/2^-)$, and $^{13}\mathrm{Be}(5/2^-)$. In positive-parity states, $^{13}\mathrm{Be}(1/2^+)$ and $^{13}\mathrm{Be}(5/2^+)$ show relatively weaker cluster structures with smaller deformations while $^{13}\mathrm{Be}(3/2^+)$ shows a remarkable 2α structure similarly to the negative-parity states.

Since an intrinsic wave function for each state is given by a Slater determinant in the AMD + VAP calculation, we can analyze single-particle wave functions and discuss neutron configurations as well as single-particle energies. Single-particle wave functions and single-particle energies of an intrinsic state are calculated by diagonalizing the single-particle Hamiltonian matrix defined by analogy to the Hartree-Fock theory as done in Refs. [15,17].

As ^{13}Be intrinsic states obtained with AMD + VAP are deformed and parity asymmetric, strictly speaking, spin and parity are not good quanta in each single-particle wave function. Nevertheless, single-particle wave functions can be associated with shell-model orbits from features of spatial distribution and ratios of positive- and negative-parity components. Figure 4 shows single-particle energies in the intrinsic wave functions of ^{13}Be states. For each single-particle level, fractions of positive and negative-parity components are shown by a red solid line and a green dotted one, respectively. Labels indicate rough correspondence to shell-model orbits. In the $^{13}\mathrm{Be}(1/2^-)$ state, the proton orbits and the lowest four neutron orbits form a 2α core. Among five valence neutrons around the 2α core, three of them occupy p-like orbits and the other two occupy sd-like orbits. Thus, the $^{13}\mathrm{Be}(1/2^-)$ roughly corresponds to a $(p)^{-1}(sd)^2$ configuration on the neutron p shell and it is regarded as a $1\hbar\omega$ excited configuration. In a similar way, also the $^{13}\mathrm{Be}(3/2^-)$ and $^{13}\mathrm{Be}(5/2^-)$ states have dominantly $(p)^{-1}(sd)^2$ configurations, and they are regarded as $1\hbar\omega$ members as well as $^{13}\mathrm{Be}(1/2^-)$. On the other hand,

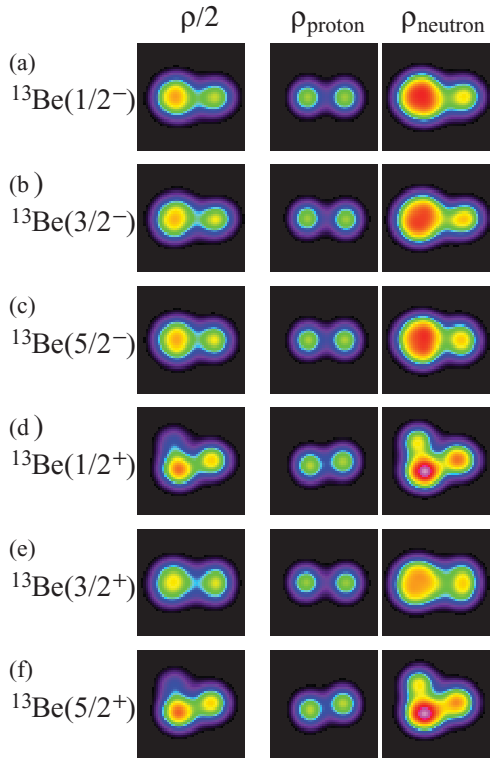

FIG. 3. (Color online) Density distributions of the intrinsic states for $1/2^-$, $3/2^-$, $5/2^-$, $1/2^+$, $3/2^+$, and $5/2^+$ states in ^{13}Be calculated with AMD + VAP using the set (1) interaction. The orientation of an intrinsic state is chosen so as to satisfy $\langle x^2\rangle \leqslant \langle y^2\rangle \leqslant \langle z^2\rangle$ and $\langle xy\rangle = \langle yz\rangle = \langle zx\rangle = 0$. The horizontal and vertical axes are set to the z and y axes, respectively. Densities are integrated with respect to the x axis. Distributions of matter, proton, and neutron densities are shown in the left, middle, and right panels, respectively.

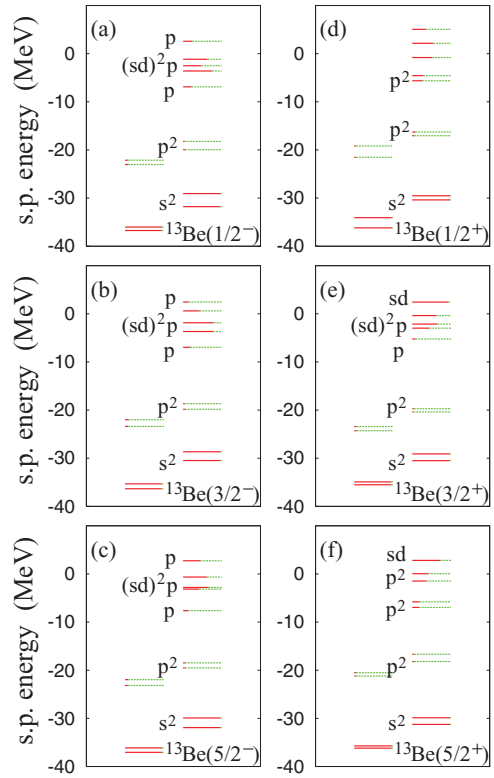

FIG. 4. (Color online) Single-particle energies in the intrinsic wave functions for ^{13}Be states, (a) $1/2^-$, (b) $3/2^-$, (c) $5/2^-$, (d) $1/2^+$, (e) $3/2^+$, (f) $5/2^+$, calculated with AMD + VAP using the set (1) interaction. Fractions of positive- and negative-parity components are shown by red solid and green dotted lines, respectively. The labels, s, p, and sd indicate association with shell-model orbits.

the ^{13}Be$(5/2^+)$ contains mainly a $(sd)^1$ configuration and corresponds to the normal $0\hbar\omega$ configuration. In contrast to the ^{13}Be$(5/2^+)$, the ^{13}Be$(3/2^+)$ contains dominantly a $2\hbar\omega$ excited configuration of a $(p)^{-2}(sd)^3$ configuration. It is surprising that $0\hbar\omega$, $1\hbar\omega$, and $2\hbar\omega$ states almost degenerate in the low-energy region in ^{13}Be.

For the ^{13}Be$(1/2^+)$ obtained with AMD + VAP, we cannot associate valence neutron wave functions with shell model orbits because parities are strongly mixing and spatial behaviors show no specific feature analogous to shell-model orbits. Furthermore, this state may not correspond to the s-wave virtual state, which has been suggested near the ^{12}Be + n threshold.

Let us compare deformations and cluster structures in ^{13}Be with those in ^{12}Be. Figures 5 and 6 show density distributions and single-particle energies of the intrinsic wave functions $\Phi(^{12}\text{Be}; 2\hbar\omega)$ for ^{12}Be(0_1^+) and $\Phi(^{12}\text{Be}; 0\hbar\omega)$ for ^{12}Be(0_2^+) obtained with AMD + VAP. As discussed in Ref. [19], ^{12}Be(0_1^+) is dominantly the $2\hbar\omega$ intruder state having a developed cluster structure with a large deformation, while ^{12}Be(0_2^+) described dominantly by the normal $0\hbar\omega$ configuration has a weaker cluster structure and a smaller deformation than those of ^{12}Be(0_1^+). It is found that the large deformations in ^{13}Be$(1/2^-)$, ^{13}Be$(3/2^-)$, ^{13}Be$(5/2^-)$, and ^{13}Be$(3/2^+)$ are similar to that of ^{12}Be(0_1^+), while smaller deformations in ^{13}Be$(1/2^+)$ and ^{13}Be$(5/2^+)$ are associated with ^{12}Be(0_2^+). Then, the ^{13}Be states can be interpreted as ^{12}Be + n states by considering an additional neutron on the ^{12}Be cores. That is, ^{13}Be$(1/2^-)$, ^{13}Be$(3/2^-)$, and ^{13}Be$(5/2^-)$ have the ^{12}Be$(2\hbar\omega)$ core with a neutron in a p orbit. ^{13}Be$(3/2^+)$ is regarded as the ^{12}Be$(2\hbar\omega)$ core and a sd-orbit neutron, while ^{13}Be$(5/2^+)$ is interpreted as the ^{12}Be$(0\hbar\omega)$ core and a sd-orbit neutron. Here the coupling of the last neutron with the ^{12}Be$(2\hbar\omega)$ core is not weak coupling but strong coupling where the neutron is moving around the largely deformed core.

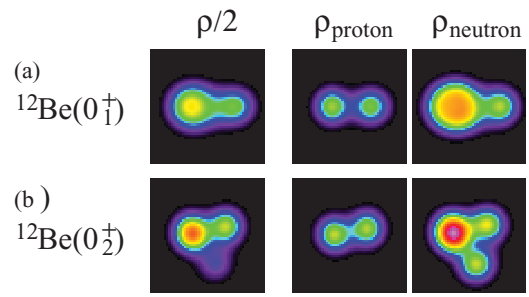

FIG. 5. (Color online) Density distributions of the intrinsic states for the 0_1^+ and 0_2^+ states of ^{12}Be calculated with AMD + VAP using the set (1) interaction. Same as Fig. 3.

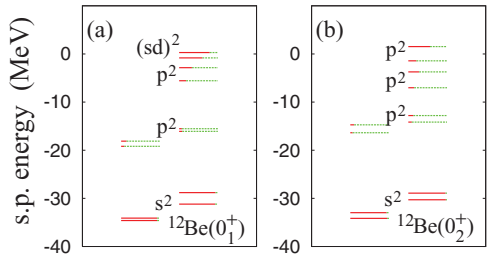

FIG. 6. (Color online) Single-particle energies in the intrinsic wave functions of ^{12}Be states. Same as Fig. 4.

The $^{12}\mathrm{Be}+n$ features in the AMD + VAP results are supported also by the $^{12}\mathrm{Be}+n$ model calculation. Indeed, in the $^{12}\mathrm{Be}+n$ model calculation, $^{13}\mathrm{Be}(1/2^-)$, $^{13}\mathrm{Be}(3/2^-)$, $^{13}\mathrm{Be}(5/2^-)$, and $^{13}\mathrm{Be}(3/2^+)$ contain mainly $^{12}\mathrm{Be}(2\hbar\omega)+n$ components, while $^{13}\mathrm{Be}(5/2^+)$ and $^{13}\mathrm{Be}(1/2^+)$ are approximately described by $^{12}\mathrm{Be}(0\hbar\omega)+n$ wave functions.

B. Assignment of calculated states to observed levels

Let us here discuss the possible assignment of calculated states to observed ^{13}Be levels. Recently, resonance states of ^{13}Be have been observed with invariant mass measurements of $^{12}\mathrm{Be}+n$ [31,32]. In the experimental work by Kondo *et al.*, a p-wave resonance at the resonance energy (the relative energy to the $^{12}\mathrm{Be}+n$ threshold) $E_r = 0.51(1)$ MeV with a width $\Gamma = 0.45(3)$ MeV and a d-wave resonance at $E_r = 2.39(5)$ MeV with $\Gamma = 2.4(2)$ MeV were reported. The J^π assignment for the former state is $J^\pi = 1/2^-$, and that for the latter state is $J^\pi = 5/2^+$. Since the width for the $5/2^+$ state is somewhat larger than the width expected from a d-wave single-particle resonance, possible contributions from other states to the spectra for the spectra around 2 MeV were discussed in Ref. [32].

As shown in the previous section, the calculated $1/2^-$ state is lower than the $5/2^+$ state, consistent with the experimental data. Although the level spacing obtained in the present calculations is much smaller than the experimental one (see Fig. 2), we consider that the $1/2^-$ and $5/2^+$ states obtained in the present calculations may correspond to the observed $1/2^-$ state at $E_r = 0.51$ MeV and the $5/2^+$ state at $E_r = 2.39$ MeV, respectively, because of structure features of these states. In the present result, the $1/2^-$ state is regarded as the state with the $^{12}\mathrm{Be}(2\hbar\omega)$ core and a neutron in a p orbit. The feature corresponds to that of the experimental $1/2^-$ state observed as a p-wave resonance in $^{12}\mathrm{Be}(0^+_1)+n$ decay spectra. The $5/2^+$ state can be interpreted as a $^{12}\mathrm{Be}(0\hbar\omega)+n$ state in a d orbit. Here we should comment on ^{12}Be structure. Even though the dominant components of the ground state and the 0^+_2 state are considered to be $0\hbar\omega$ and $2\hbar\omega$ configurations, respectively, these configurations actually mix to each other in the $^{12}\mathrm{Be}(0^+_1)$ and $^{12}\mathrm{Be}(0^+_2)$ states. The mixing is significant as discussed, for instance, in Ref. [49]. Via the mixing of $0\hbar\omega$ and $2\hbar\omega$ components, the $5/2^+$ state may decay to $^{12}\mathrm{Be}(0^+_1)+n$ as well as $^{12}\mathrm{Be}(0^+_2)+n$. Considering the phase space, the $^{12}\mathrm{Be}(0^+_1)+n$ decay can be favored for the $5/2^+$ state. Therefore, the calculated $5/2^+$ state seems consistent with the experimental $5/2^+$ state observed as a d-wave resonance in $^{12}\mathrm{Be}(0^+_1)+n$ spectra.

As for the $3/2^+$ state, the $3/2^+$ state having the structure with the $^{12}\mathrm{Be}(2\hbar\omega)$ core and a neutron in a sd orbit is predicted near or above the $5/2^+$ state in the present calculations. This state mainly contains a $(p)^{-2}(sd)^3$ configuration. In knock-out reactions from ^{14}Be performed in Refs. [31,32], the production of such the exotic configurations with three neutrons in sd orbits might be suppressed in general. However, because of possible configuration mixing in $^{14}\mathrm{Be}(0^+_1)$ and $^{13}\mathrm{Be}(3/2^+)$, there may be a chance to observe a weak signal for the $3/2^+$ state. In this case, the $3/2^+$ state contribution might be contained in d-wave components in $^{12}\mathrm{Be}(0^+_1)+n$ spectra.

Unfortunately, the predictive power of the present calculations is not sufficient to discuss the precise structure of energy levels. As shown in the previous section, the present calculations still have model dependence as well as effective interaction dependence. Further improvements of calculations are required to predict precise energy positions.

C. Molecular orbital picture

In theoretical works on cluster structures of Be isotopes [8–29], low-lying states of ^{9}Be, ^{10}Be, ^{11}Be, and ^{12}Be have been successfully described in terms of molecular orbitals around a 2α core. As mentioned, the present work suggests the 2α core formation in ^{13}Be as well as in other Be isotopes. We here extend the molecular orbital description to ^{13}Be and discuss structures of Be isotopes systematically.

In the molecular orbital picture for a 2α system, molecular orbitals are formed by a linear combination of p orbits around two α clusters, and valence neutrons occupy the molecular orbitals around the 2α core [8–13]. A negative-parity orbital constructed by p-orbits perpendicular to the α-α direction is called a "π orbital", and a positive-parity orbital from p orbits parallel to the α-α direction is called a "σ orbital" [Fig. 7(a) and 7(b)]. We call the other positive-party orbital given by p orbits perpendicular to the α-α direction a "π^* orbital" in analogy to electron orbitals in atomic molecular systems [Fig. 7(c)].

To understand the breaking of magicity in a chain of Be isotopes, single-particle levels in the molecular orbital model (MO levels) is useful as discussed, for instance, in Ref. [12]. In the molecular orbital models [9–12], single-particle levels are evaluated as functions of the α-α distance. They are smoothly connected from the one-center limit to the two-center limit, and those in the intermediate region correspond to molecular orbitals. In addition to the spatial configurations (π, σ, and π^*), molecular orbitals are specified by the angular momentum $\Omega \equiv j_z$ projected on to the symmetric axis z. For the σ orbital, $\Omega = 1/2$, and we use the notation $\sigma_{1/2}$. For π and π^* orbitals, $\Omega = 1/2$ and $3/2$ are possible. Due to the spin-orbit force, π orbitals split into the ls-favored $\pi_{3/2}$ orbital and the ls-unfavored $\pi_{1/2}$ orbital, and $\pi^*_{3/2}$ orbitals split into the $\pi^*_{3/2}$ and $\pi^*_{1/2}$ orbitals. Note that the present notations, $\pi_{3/2}$, $\pi_{1/2}$, $\sigma_{1/2}$, and $\pi^*_{3/2}$ correspond to the labels $\pi 3/2^-(g)$, $\sigma 1/2^-(g)$, $\sigma 1/2^+(u)$, and $\pi 3/2^+(u)$ in Fig. 15 of Ref. [12], and the labels $(3u, 1)$, $(1u, 2)$, $(1g, 2)$, and $(1g, 2)$ in Ref. [9], respectively. In the spherical shell model limit, the $\pi_{3/2}$ and $\pi_{1/2}$ orbitals lead

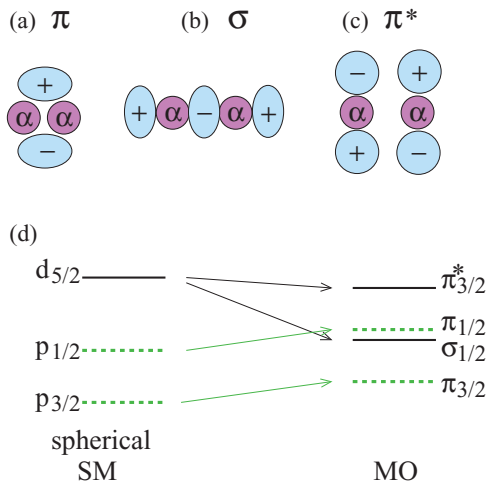

FIG. 7. (Color online) (a)–(c) Schematic figures for molecular orbitals around a 2α core. (d) A schematic figure for evolution of single-particle level ordering from spherical shell-model levels to molecular orbital levels.

to the $p_{3/2}$ and $p_{1/2}$ orbits, respectively, while the $\sigma_{1/2}$ and $\pi^*_{3/2}$ orbitals lead to the $d_{5/2}$ orbit. The MO levels correspond well to the single-particle levels in the two-center shell model [50]. Moreover, when a α-α distance is not large, the MO levels are associated with the Nilsson levels of the deformed shell model [30].

One of the important features of molecular orbitals is that the σ orbital has two nodes along the α-α direction and it gains kinetic energy as the 2α cluster develops. The breaking of $N = 8$ magicity in ^{11}Be and ^{12}Be is understood by the energy gain of the $\sigma_{1/2}$ orbital in developed 2α systems.

Let us describe structures of ^{13}Be with a 2α core and five valence neutrons in terms of molecular orbitals. In the developed cluster states of ^{13}Be obtained with AMD + VAP, neutron wave functions are associated with molecular orbitals. For instance, in the $1/2^-$ state, three neutron wave functions correspond to the π orbital and two neutron orbitals are associated with the σ orbital. This state is described by a molecular configuration, $\pi^2_{3/2}\pi^1_{1/2}\sigma^2_{1/2}$. In a similar way, the $3/2^+$ state is understood by a $\pi^2_{3/2}\sigma^2_{1/2}\pi^*_{3/2}$ configuration. In both cases, two neutrons occupy the $\sigma_{1/2}$ orbital. Then, the reason for the low-lying intruder states in ^{13}Be can be understood again by the lowering $\sigma_{1/2}$ orbital in the developed cluster structures. In other words, $\sigma_{1/2}$-orbital neutrons play an important role for the breaking of $N = 8$ magicity in ^{13}Be as well as ^{12}Be. As for the $5/2^+$ state in ^{13}Be, since it has a weaker cluster structure and a smaller deformation, its neutron configurations should be associated with spherical shell-model orbits rather than molecular orbitals. Nevertheless, taking into account the correspondence of the $\pi_{3/2}$, $\pi_{1/2}$, and $\sigma_{1/2}$ orbitals to the $p_{3/2}$, $p_{1/2}$, and $d_{5/2}$ orbits, we here temporarily assign "$\pi^2_{3/2}\pi^2_{1/2}\sigma^1_{1/2}$" to the $5/2^+$ state in the following discussion.

Energy spectra of Be isotopes can be understood systematically according to the ordering of MO levels. In the MO level ordering, the key feature is that such the orbitals as σ and π^* orbitals with nodal structures parallel to the 2α direction gain kinetic energy in a developed 2α system. As mentioned, the σ orbital with two nodes gains the energy as the cluster develops. Also the π^* orbitals with one node gain some kinetic energy in a developed cluster system. Differently from the σ and π^* orbitals, the π orbitals have no node and their energies increase relatively. Consequently, as the 2α cluster develops, the ordering of single-particle levels changes from spherical shell model orbits as shown in Fig. 7(d). In this scenario, the breaking of the neutron magicity in Be isotopes occurs due to the intruder $\sigma_{1/2}$ orbital which comes down below the $\pi_{1/2}$ orbital in the developed 2α systems. As a result, the $N = 8$ shell gap disappears and the level ordering based on a spherical shell model picture is no longer valid in neutron-rich Be. Instead, the level ordering of molecular orbitals works rather well to understand the energy spectra of Be isotopes. From the fact that ^{11}Be$(1/2^+)$ and ^{11}Be$(1/2^-)$ almost degenerate, one may expect, in the first-order approximation, that the $\pi_{1/2}$ and $\sigma_{1/2}$ orbitals almost degenerate in the MO levels. In the new ordering of the MO levels on a 2α core, the $\pi_{3/2}$ orbital should be the lowest, $\sigma_{1/2}$ and $\pi_{1/2}$ orbitals compose the second group (called a $\sigma_{1/2}$-$\pi_{1/2}$ shell in the present paper), and the $\pi^*_{3/2}$ orbital may exist above them [Fig. 7(d)].

Let us review the molecular orbital configurations of Be isotopes. In Table I, configurations for valence neutrons around a 2α core for band-head states of Be isotopes are summarized. For ^{10}Be, ^{10}Be(0^+_1), ^{10}Be(1^-), and ^{10}Be(0^+_2) are described by the valence neutron configurations of $\pi^2_{3/2}$, $\pi_{3/2}\sigma_{1/2}$, and $\sigma^2_{1/2}$ meaning two neutrons in the π orbital, one neutron in the $\pi_{3/2}$ orbital and the other neutron in the $\sigma_{1/2}$ orbital, and two neutrons in the $\sigma_{1/2}$ orbital, respectively. In a similar way, ^{11}Be$(1/2^+)$,^{11}Be$(1/2^-)$, and ^{11}Be$(3/2^-_2)$ states are described by $\pi^2_{3/2}\sigma_{1/2}$, $\pi^2_{3/2}\pi^1_{1/2}$, and $\pi^1_{3/2}\sigma^2_{1/2}$ configurations,

TABLE I. Classification of band-head states in $^{10-14}$Be. Harmonic oscillator shell-model configurations and molecular orbital configurations are listed. The shell model configurations $0\hbar\omega$, $1\hbar\omega$, and $2\hbar\omega$ are based on neutrons excited from the p shell to sd shell. For molecular orbital configurations, neutron configurations around a 2α core are described. The numbers of $\pi_{3/2}$ holes and $\pi^*_{3/2}$ particles are also shown. The molecular orbital configuration for ^{13}Be$(5/2^+)$ is a temporary assignment (see text).

	H.O.	M.O.		
	excitation	config.	$\pi_{3/2}$ holes	$\pi^*_{3/2}$ particles
^{10}Be(0^+_1)	$0\hbar\omega$	$\pi^2_{3/2}$	0	0
^{10}Be(1^-)	$1\hbar\omega$	$\pi_{3/2}\sigma_{1/2}$	1	0
^{10}Be(0^+_2)	$2\hbar\omega$	$\sigma^2_{1/2}$	2	0
^{11}Be$(1/2^+)$	$1\hbar\omega$	$\pi^2_{3/2}\sigma_{1/2}$	0	0
^{11}Be$(1/2^-)$	$0\hbar\omega$	$\pi^2_{3/2}\pi_{1/2}$	0	0
^{11}Be$(3/2^-)$	$2\hbar\omega$	$\pi_{3/2}\sigma^2_{1/2}$	1	0
^{12}Be(0^+_1)	$2\hbar\omega$	$\pi^2_{3/2}\sigma^2_{1/2}$	0	0
^{12}Be(0^+_2)	$0\hbar\omega$	$\pi^2_{3/2}\pi^2_{1/2}$	0	0
^{12}Be(1^-)	$1\hbar\omega$	$\pi^2_{3/2}\pi_{1/2}\sigma_{1/2}$	0	0
^{13}Be$(1/2^-)$	$1\hbar\omega$	$\pi^2_{3/2}\pi_{1/2}\sigma^2_{1/2}$	0	0
^{13}Be$(5/2^+)$	$0\hbar\omega$	$(\pi^2_{3/2}\pi^2_{1/2}\sigma_{1/2})$	0	0
^{13}Be$(3/2^+)$	$2\hbar\omega$	$\pi^2_{3/2}\sigma^2_{1/2}\pi^*_{3/2}$	0	1
^{14}Be(0^+_1)	$0\hbar\omega$	$\pi^2_{3/2}\pi^2_{1/2}\sigma^2_{1/2}$	0	0
^{14}Be(0^+_2)	$2\hbar\omega$	$\pi^2_{3/2}\sigma^2_{1/2}\pi^{*2}_{3/2}$	0	2

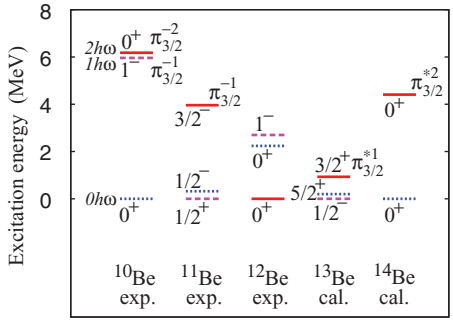

FIG. 8. (Color online) Excitation energies of band-head states in $^{10-14}$Be. Experimental data are shown for $^{10-12}$Be, and theoretical values for ^{14}Be [51] are shown. The data for ^{13}Be are the present results obtained by the ^{12}Be-n model calculation. Blue dotted, magenta dashed, and red solid lines indicate $0\hbar\omega$, $1\hbar\omega$, and $2\hbar\omega$ configuration states, respectively.

while ^{12}Be(0^+_1), ^{12}Be(0^+_2), and ^{12}Be(1^-_1) states correspond to $\pi^2_{3/2}\sigma^2_{1/2}$, $\pi^2_{3/2}\pi^2_{1/2}$, and $\pi^2_{3/2}\pi^1_{1/2}\sigma^1_{1/2}$, respectively. These assignments have been suggested by molecular orbital models [12,13], cluster models [22,23,26–28], and also the AMD model [15,17–19]. For ^{13}Be, the molecular orbital configurations, $\pi^2_{3/2}\pi^1_{1/2}\sigma^2_{1/2}$ and $\pi^2_{3/2}\sigma^2_{1/2}\pi^{*1}_{3/2}$, are assigned to ^{13}Be$(1/2^-)$ and ^{13}Be$(3/2^+)$, respectively, and $\pi^2_{3/2}\pi^2_{1/2}\sigma^1_{1/2}$ is temporarily assigned to ^{13}Be$(5/2^+)$, as mentioned. For ^{14}Be, the ground state ^{14}Be(0^+_1) is considered to be a $\pi^2_{3/2}\pi^2_{1/2}\sigma^2_{1/2}$ configuration. An excited 0^+_2 band was theoretically suggested by a VAP calculation [51] and a $\pi^2_{3/2}\sigma^2_{1/2}\pi^{*2}_{3/2}$ configuration was assigned.

Finally, we discuss energy spectra of Be isotopes in relation with molecular orbital configurations. In Fig. 8, experimental excitation energies are shown for $^{10-12}$Be, while theoretical values are shown for ^{13}Be and ^{14}Be [51]. In terms of spherical shell model levels, the inversion between $0\hbar\omega$, $1\hbar\omega$, and $2\hbar\omega$ occurs in $^{11-13}$Be, and the energy spectra seem to be out of the normal ordering. However, in terms of MO levels, the energy spectra of Be isotopes can be understood rather easily. In MO levels, the neutron Fermi level exists at the $\sigma_{1/2}$-$\pi_{1/2}$ shell in $^{10-14}$Be. Excited configurations are characterized by $\pi_{3/2}$-orbital holes or $\pi^*_{3/2}$-orbital particles. Configurations without $\pi^*_{3/2}$ particles nor $\pi_{3/2}$ holes are normal in the MO levels and they degenerate in a low-energy region. For instance, the degeneracy of ^{11}Be$(1/2^+)$ and ^{11}Be$(1/2^-)$ can be understood because all these states have "normal" configurations in MO levels. Also the coexistence of ^{12}Be(0^+_1), ^{12}Be(0^+_2), and ^{12}Be(1^-) in the low-energy region is to be expected because they have no excitation in MO configurations. In a similar way, the coexistence of ^{13}Be$(1/2^-)$ and ^{13}Be$(5/2^+)$ is not surprising as they have normal MO configurations. Excited configuration states with $\pi_{3/2}$ holes or $\pi^*_{3/2}$ particles have generally higher excitation energies than low-lying normal MO configuration states. The numbers of $\pi_{3/2}$ holes and $\pi^*_{3/2}$ particles are noted in Fig. 8 as well as Table I. ^{10}Be(0^+_2), ^{10}Be(1^-), ^{10}Be(0^+_2), and ^{11}Be$(3/2^-)$ have one or two $\pi_{3/2}$ holes, and they exist in the excitation energy region around $E_x = 4 \sim 6$ MeV. The excited state with a $\pi^*_{3/2}$ particle and that with two $\pi^*_{3/2}$ particles are suggested in ^{13}Be$(3/2^+)$ and ^{14}Be(0^+_2), respectively. For more detailed discussion of energy spectra, one should take into account two-body correlations and α-α distance dependence of those MO levels.

V. SUMMARY

Structure of ^{13}Be was investigated with VAP+AMD. In the AMD + VAP calculation using the set (1) interaction that reproduces the parity inversion of ^{11}Be, an unnatural parity $1/2^-$ state was suggested to be lower than $5/2^+$ state indicating that the vanishing of $N = 8$ magic number occurs in ^{13}Be. A low-lying $3/2^+$ state with a $2\hbar\omega$ configuration was also suggested. The present AMD + VAP calculation is a bound state approximation. To see effects of spatial extension of the last neutron wave function on the energy spectra, we also calculated ^{13}Be in the ^{12}Be + n model. The degeneracy of the $1/2^-$, $5/2^+$, and $3/2^+$ states was suggested also by the ^{12}Be + n model calculation.

In analysis of intrinsic structures of ^{13}Be, large deformations with developed cluster structures are found in the intruder states such as the $1/2^-$ and $3/2^+$ states. These deformed states are regarded as states composed by one neutron on the deformed ^{12}Be core, which corresponds to the intrinsic state of ^{12}Be(0^+_1).

The intrinsic structures of ^{13}Be were also discussed in terms of molecular orbitals around a 2α core. The intruder states, ^{13}Be$(1/2^-)$ and ^{13}Be$(3/2^+)$ are described by the molecular configurations, $\pi^2_{3/2}\pi^1_{1/2}\sigma^2_{1/2}$ and $\pi^2_{3/2}\sigma^2_{1/2}\pi^{*1}_{3/2}$, respectively. The breaking of $N = 8$ magicity in ^{13}Be can be understood by molecular orbital levels as well as ^{11}Be and ^{12}Be.

Based on the obtained energy levels and analysis of intrinsic structures, we assigned the calculated $1/2^-$ and $5/2^+$ states to the observed $1/2^-$ state at $E_r = 0.51$ MeV and the $5/2^+$ state at $E_r = 2.39$ MeV reported by Kondo *et al.* [32]. Unfortunately, the predictive power of the present calculations is not sufficient to discuss the precise structure of energy levels. For instance, the level spacing between the $1/2^-$ and $5/2^+$ states in the present calculations is much smaller than the experimental one. The present calculations still have the model dependence as well as the effective interaction dependence. Further improvements of calculations are required to predict precise energy positions. It is also necessary to treat asymptotic behaviors and out-going boundary more carefully to discuss detailed energy spectra, in particular, for low-spin resonances.

[1] T. Suzuki and T. Otsuka, Phys. Rev. C **56**, 847 (1997).
[2] H. Iwasaki *et al.*, Phys. Lett. B **481**, 7 (2000).
[3] H. Iwasaki *et al.*, Phys. Lett. B **491**, 8 (2000).
[4] A. Navin *et al.*, Phys. Rev. Lett. **85**, 266 (2000).
[5] S. Shimoura *et al.*, Phys. Lett. B **560**, 31 (2003).
[6] S. D. Pain *et al.*, Phys. Rev. Lett. **96**, 032502 (2006).

[7] H. Simon *et al*. Phys. Rev. Lett. **83**, 496 (1999).
[8] S. Okabe, Y. Abe, and H. Tanaka, Prog. Theor. Phys. **57**, 866 (1977); S. Okabe and Y. Abe, *ibid*. **59**, 315 (1978); **61**, 1049 (1979).
[9] M. Seya, M. Kohno, and S. Nagata, Prog. Theor. Phys. **65**, 204 (1981).
[10] W. von Oertzen, Z. Phys. A **354**, 37 (1996); **357**, 355 (1997).
[11] W. von Oertzen, Nuovo Cimento **110**, 895 (1997).
[12] W. von Oertzen, M. Freer, and Y. Kanada-En'yo, Phys. Rep. **432**, 43 (2006).
[13] N. Itagaki and S. Okabe, Phys. Rev. C **61**, 044306 (2000); N. Itagaki, S. Okabe, and K. Ikeda, *ibid*. **62**, 034301 (2000).
[14] Y. Kanada-Enyo, H. Horiuchi, and A. Ono, Phys. Rev. C **52**, 628 (1995); Y. Kanada-Enyo and H. Horiuchi, *ibid*. **52**, 647 (1995).
[15] A. Dote, H. Horiuchi, and Y. Kanada-En'yo, Phys. Rev. C **56**, 1844 (1997).
[16] Y. Kanada-En'yo and H. Horiuchi, Prog. Theor. Phys. Suppl. **142**, 205 (2001); Y. Kanada-En'yo, M. Kimura, and H. Horiuchi, C. R. Physique **4**, 497 (2003); Y. Kanada-En'yo and M. Kimura, Lect. Notes Phys. **818**, 129 (2010); Prog. Theor. Exp. Phys. (to be published).
[17] Y. Kanada-En'yo, H. Horiuchi, and A. Doté, Phys. Rev. C **60**, 064304 (1999).
[18] Y. Kanada-En'yo and H. Horiuchi, Phys. Rev. C **66**, 024305 (2002).
[19] Y. Kanada-En'yo and H. Horiuchi, Phys. Rev. C **68**, 014319 (2003).
[20] K. Arai, Y. Ogawa, Y. Suzuki, and K. Varga, Phys. Rev. C **54**, 132 (1996).
[21] Y. Ogawa, K. Arai, Y. Suzuki, and K. Varga, Nucl. Phys. A **673**, 122 (2000).
[22] K. Arai, Y. Ogawa, Y. Suzuki, and K. Varga, Prog. Theor. Phys. Suppl. **142**, 97 (2001).
[23] K. Arai, Phys. Rev. C **69**, 014309 (2004).
[24] P. Descouvemont and D. Baye, Phys. Lett. B **505**, 71 (2001).
[25] P. Descouvemont, Nucl. Phys. A **699**, 463 (2002).
[26] M. Ito, K. Kato, and K. Ikeda, Phys. Lett. B **588**, 43 (2004).
[27] M. Ito, Phys. Lett. B **636**, 293 (2006).
[28] M. Ito, N. Itagaki, H. Sakurai, and K. Ikeda, Phys. Rev. Lett. **100**, 182502 (2008).
[29] M. Ito, N. Itagaki, and K. Ikeda, Phys. Rev. C **85**, 014302 (2012).
[30] A. Bohr and B. R. Mottelson, *Nuclear Structure*, Vol. II (Benjamin, New York, 1975).
[31] H. Simon *et al*., Nucl. Phys. A **791**, 267 (2007).
[32] Y. Kondo *et al*., Phys. Lett. B **690**, 245 (2010).
[33] A. N. Ostrowski, Z. Phys. A **343**, 489 (1992).
[34] A. A. Korsheninnikov *et al*., Phys. Lett. B **343**, 53 (1995).
[35] A. V. Belozerov *et al*., Nucl. Phys. A **636**, 419 (1998).
[36] M. Thoennessen, S. Yokoyama, and P. G. Hansen, Phys. Rev. C **63**, 014308 (2000).
[37] H. Simon *et al*., Nucl. Phys. A **734**, 323 (2004).
[38] J. L. Lecouey (LPC-CHARISSA-DEMON Collaboration), Few-Body Syst. **34**, 21 (2004).
[39] H. Al Falou, A. Leprince, and N. A. Orr, arXiv:1004.3233 [nucl-ex].
[40] H. T. Fortune and R. Sherr, Phys. Rev. C **82**, 064302 (2010).
[41] M. Labiche, F. M. Marqués, O. Sorlin, and N. Vinh Mau, Phys. Rev. C **60**, 027303 (1999).
[42] T. Suzuki, R. Fujimoto, and T. Otsuka, Phys. Rev. C **67**, 044302 (2003).
[43] P. Descouvemont, Phys. Lett. B **331**, 271 (1994); Phys. Rev. C **52**, 704 (1995).
[44] Y. Kanada-Enyo and H. Horiuchi, Prog. Theor. Phys. **93**, 115 (1995).
[45] Y. Kanada-En'yo, Phys. Rev. Lett. **81**, 5291 (1998); Prog. Theor. Phys. **117**, 655 (2007).
[46] T. Ando, K. Ikeda, and A. Tohsaki, Prog. Theor. Phys. **64**, 1608 (1980).
[47] N. Yamaguchi, T. Kasahara, S. Nagata, and Y. Akaishi, Prog. Theor. Phys. **62**, 1018 (1979); R. Tamagaki, *ibid*. **39**, 91 (1968).
[48] J. H. Kelley, E. Kwan, J. E. Purcell, C. G. Sheu, and H. R. Weller, Nucl. Phys. A **880**, 88 (2012).
[49] M. Takashina and Y. Kanada-En'yo, Phys. Rev. C **77**, 014604 (2008).
[50] J. M. Eisenberg and W. Greiner, *Nuclear Theory 1, Nuclear Models* (Elsevier Science Publishers, Amsterdam, 1985).
[51] Y. Kanada-En'yo, Phys. Rev. C **66**, 011303(R) (2002).